Proceedings of the ASME 2019 38th International Conference on Ocean, Offshore and Arctic Engineering
OMAE2019
June 9-14, 2019, Glasgow, Scotland, UK

OMAE2019-96346

WAVE EFFECTS ON THE TURNING ABILITY OF AN ULTRA LARGE CONTAINER SHIP IN SHALLOW WATER

Manases Tello Ruiz[1], Marc Mansuy, Luca Donatini
Ghent University
Ghent, Belgium

Jose Villagomez
Flanders Hydraulics Research
Antwerp, Belgium

Guillaume Delefortrie
Flanders Hydraulics Research
Antwerp, Belgium
Ghent University
Ghent, Belgium

Evert Lataire, Marc Vantorre
Ghent University
Ghent, Belgium

ABSTRACT

The influence of waves on ship behaviour can lead to hazardous scenarios which put at risk the ship, the crew and the surroundings. For this reason, investigating the effect of waves on manoeuvring is of relevant interest. Waves may impair the overall manoeuvring performance of ships hence increasing risks such as collisions, which are of critical importance when considering dense traffic around harbour entrances and in unsheltered access channels. These are conditions met by Ultra Large Container Ships (ULCS) when approaching a port, e.g. in the North Sea access channels to the main sea ports of Belgium. Note that due to the large draft of ULCS and the limited water depth, shallow water effects will also influenced the ship. Thus, in such scenarios the combined effects of shallow water and waves on the ship's manoeuvring need to be studied.

The present work investigates the effect of waves on the turning ability of an ULCS in shallow water. Simulations are carried out using the two time scale approach. The restricted water depth corresponds to 50% Under Keel Clearance (UKC). To gain a better insight on the forces acting on the ship, the propulsion, and the rudder behaviour in waves experimental studies were conducted. These tests were carried out in the Towing Tank for Manoeuvres in Confined Water at Flanders Hydraulics Research (in co-operation with Ghent University) with a scale model of an ULCS. Different wave lengths, wave amplitudes, ships speeds, propeller rates, and rudder angles were tested. The turning ability characteristics obtained from simulations in waves and calm water are presented, and discussed.

Keywords: Manoeuvring in waves, shallow water, turning ability.

INTRODUCTION

An accurate prediction of the ship behaviour has always been of major interest in order to foresee hazardous scenarios. One of the topics of interest is the manoeuvring problem of a ship in waves. The lack of a well-defined method to solve this problem has boosted research in this field. Some examples of works addressing this problem are, [1], [2], [3], [4] and more recently [5] [6], and [7] among others.

From literature, two types of approaches can be identified, the unified method, e.g. [1], and a parallel marching scheme known as the two time scale method, e.g. [2].

The unified method is relatively complex as it aims to merge the gained knowledge in the fields on manoeuvring in calm water and seakeeping. For instance in [1] the authors combine the influence of memory effects and viscous effects on the hull in a more general memory function. The major disadvantage of this method lies in its complexity and in the difficulty to incorporate other sources of forces, for instance due to vorticity at the stern of the ship. Another major constraint is that its application to shallow water conditions, where other fluid phenomena such as squat effects, are not yet properly addressed. In [7] a first attempt has been proposed to use the unified method for shallow water, but yet it requires additional considerations and further study.

The two time scale method solves the manoeuvring problem in waves by splitting the problem in two sub modules, a manoeuvring module (MM), developed for calm water, and a seakeeping module (SM). Both of these modules are solved independently and coupled in a parallel marching scheme; where information is shared between the modules. The MM accounts for the hull, rudder, and propeller forces, as in calm water, while the SM accounts for the mean second order wave forces only.

[1]Contact author: Manases.ruiz@UGent.be

The variables exchanged between the modules are, ship speed, and heading from the MM to the SM model, and wave forces from the SM to the MM model. The two modules can run with different time steps, which is usually the common practice to save computational time.

In the present study, the two time scale model to investigate the problem of manoeuvring in waves was preferred over the unified method because of its simplicity and direct application. It is important to mention that as the main goal of the present study is to investigate the effect of waves on the turning ability the analysis is restricted to the horizontal plane. Hence, squat and the ship oscillatory vertical motions are not considered.

In the present study, model tests have been conducted to investigate, more accurately, the effect of waves on the hull forces, and on the propeller and rudder performances. The experimental program was carried out in the Towing Tank for Manoeuvres in Confined Water at Flanders Hydraulics Research (in co-operation with Ghent University) with a 1/90 scale model of an ULCS

Note that in the present study a numerical analysis was also conducted with the software package HydroStar [8] to fill the gaps where experimental research was not possible.

THE MATHEMATICAL MODEL

Coordinate System and General Definitions

During tests, the ship's position and orientation along the tank are defined by using two coordinate systems, an Earth-fixed coordinate system ($O_0 - x_0\ y_0\ z_0$) and a body-fixed coordinate system ($O - xyz$); both are North-East-Down (NED) oriented. The longitudinal $x-$axis for the body-fixed system is aligned with the ship's centreline, positive towards the bow and parallel to the longitudinal axes of the Earth-fixed system at rest.

To define the ship's relative orientation during tests in waves, parameters such as wave angle of encounter (μ), hull drift angle (β), and ship's heading angle (ψ) are used. The wave direction with the y_0-axis defines the angle η

Modular Approach

To study ship manoeuvring, the equations of motion governing the ship's rigid body motions in six degrees of freedom need to be defined first. The equations of motion are expressed in the $O - xyz$ axes system, of which the origin is fixed amidships.

The forces are modelled using the modular approach as:

$$\boldsymbol{F} = \boldsymbol{F_H} + \boldsymbol{F_P} + \boldsymbol{F_R} + \boldsymbol{F_W} \tag{1}$$

where the subscripts H, P, R, and W indicate hull, propeller, rudder, and wave contributions.

Hull Forces

The model considers a three degrees of freedom (DoF) analysis and is based on the mathematical models developed in [9]. Heave, roll and pitch motions are neglected from the analysis as the main goal is to investigate the effect of waves in the ship's turning ability. The hull forces are given as:

$$\begin{bmatrix} X_H \\ Y_H \\ N_H \end{bmatrix} = \frac{\rho}{2} L_{PP}^{s} T_m \begin{bmatrix} X'^{(\beta)} & X'^{(\gamma)} & X'^{(\chi)} \\ Y'^{(\beta)} & Y'^{(\gamma)} & Y'^{(\chi)} \\ N'^{(\beta)} & N'^{(\gamma)} & N'^{(\chi)} \end{bmatrix} \begin{bmatrix} u^2 + v^2 \\ u^2 + v_{\mathrm{P}}^2 \\ v^2 + v_{\mathrm{P}}^2 \end{bmatrix} + \begin{bmatrix} X_{\dot{u}} \\ Y_{\dot{v}} \\ N_{\dot{v}} \end{bmatrix}^T \begin{bmatrix} \dot{u} \\ \dot{v} \\ \dot{v} \end{bmatrix} + \begin{bmatrix} 0 \\ Y_{\dot{r}}^{(\beta)} \\ N_{\dot{r}}^{(\beta)} \end{bmatrix} \dot{r} \tag{2}$$

where ρ, L_{PP}, and T_m are the water density, the ship's length between perpendicular and amidships draft, respectively. The exponent s takes the value of 1 for the forces (X_H, Y_H), and 2 for the yaw moment N_H. u and v, stand for the ship's longitudinal and lateral velocity, respectively, and the reference lateral velocity v_{P} due to yaw is given by:

$$v_{\mathrm{P}} = rL_{PP}/2 \tag{3}$$

r being the ship's yaw angular velocity. The upper dots indicate time derivatives.

In Eq. (2) β, γ, χ refer to the hydrodynamic angles which are defined by:

$$\beta = \arctan\left(\frac{-v}{u}\right) \tag{4}$$

$$\gamma = \arctan\left(\frac{v_P}{u}\right) \tag{5}$$

$$\chi = \arctan\left(\frac{v_P}{v}\right) \tag{6}$$

In Eq. (2) the nine terms multiplying the square of the velocities, $X'^{(\beta)}$ to $N'^{(\chi)}$, are tabular coefficients expressed as functions of the hydrodynamic angles β, γ, and χ. They express phenomena such as lift, drag, and cross flow effects which are relevant for the horizontal forces and moments. The terms proportional to accelerations are the added masses and moment of inertia. Note, however, that in the current approach the sway added mass, $Y_{\dot{r}}(\beta)$ and the yaw added moment of inertia $N_{\dot{r}}(\beta)$ are also tabular functions but depend only of the drift angle β.

Propeller Forces

Manoeuvring models for full bridge simulations include positive and negative ship longitudinal speeds u and propeller rates n, the combination of which yield to four possible arrangements known as quadrants. The first quadrant corresponds to positive u speeds and n rates. The present work

focuses only on the first quadrant as only positive values for u and n are experienced during the turning circle tests.

The longitudinal force (X_P) on the hull due to the propeller action is expressed as function of the propeller thrust (T) and the thrust deduction factor (t).

$$X_P = (1-t)T \tag{7}$$

The thrust deduction factor is generally understood as an increase of the ship's resistance due to the presence of the working propeller. t can be obtained experimentally and is given as a function of the apparent advance number J_A.

$$J_A = \frac{u}{nD} \tag{8}$$

In literature, it is also common to express t as a function of the hydrodynamic advance angle ε, defined by:

$$\varepsilon_A = \arctan\left(\frac{J_A}{0.7\pi}\right) \tag{9}$$

The thrust T is a function of the square of the propeller rate (n) and the thrust coefficient (K_T).

$$T = \rho D^4 \, n^2 K_T \tag{10}$$

In Eq. (9) D is the propeller diameter and ρ the water density. The thrust coefficient K_T is given as function of the advance number J, defined as:

$$J = \frac{u(1-w_T)}{nD} \tag{11}$$

where w_T is the wake fraction which indicates the free flow speed u reduction at the location of the propeller due to the presence of the ship.

The wake fraction, as the thrust deduction factor, is expressed as function of the apparent advance number J_A.

The lateral force and yaw moment due to the propeller action are in general small. Therefore, in the present study they have been omitted as in [10]. Other authors, however, still account for them, e.g. [11] and [12]. This will be considered in further studies.

Rudder Forces

Rudder forces can be obtained by combining the lift (C_{LR}) and the drag coefficients (C_{DR}) of the rudder, the inflow velocity V_R, the inflow angle α_R, and the rudder angle δ_R as:

$$\begin{bmatrix} F_X \\ F_Y \end{bmatrix} = \frac{1}{2}\rho A_P V_R^2 \begin{bmatrix} -cos\beta_R & sin\beta_R \\ sin\beta_R & cos\beta_R \end{bmatrix} \begin{bmatrix} C_{DR} \\ C_{LR} \end{bmatrix} \tag{12}$$

In Eq. (12) C_{LR} and C_{DR} are functions of the inflow angle α_R, defined by:

$$\alpha_R = \delta_R + \delta_0 + \beta_R \tag{13}$$

where δ_0 is a flow asymmetry correction (see, [13]) defined at the condition where the normal force to the rudder vanishes. In Eq. (12) and (13) β_R is the local drift angle given by:

$$\beta_R = \arctan\left(\frac{-v_R}{u_R}\right) \tag{14}$$

where u_R and v_R are the longitudinal and lateral speed components of V_R, v_R is given by:

$$v_R = k_{HR}(v + r x_R) \tag{15}$$

The variables k_{HR} and x_R refer to the straightening coefficient and the longitudinal position of the rudder axis. More details on these parameters can be found in [14].

u_R is estimated by a weighted average of the free flow u_{R0} and the flow due to the propeller action u_{RP}, see Eq. (16).

$$u_R = \sqrt{\eta^* u_{RP}^2 + (1-\eta^*)u_{R0}^2} \tag{16}$$

The velocity u_{R0}, is given by u and the wake fraction w_R:

$$u_{R0} = u(1-w_R) \tag{17}$$

In Eq. (16) η^* is the propeller diameter D to rudder height H_R ratio ($\eta^* = D/H_R$), and u_{RP} is estimated based on the momentum theory [15] as:

$$u_{RP} = u_{R0} + K_m u_P \left(\sqrt{1 + \frac{8K_T}{\pi J^2}} - 1\right) \tag{18}$$

where u_P is the inflow velocity at the propeller and K_m is a factor taking into account the propeller jet contraction at the rudder location. K_m can vary between 0.5 to 0.96 according to [15], and is given as function of the distance between the rudder stock and the propeller blade tips.

Finally the rudder longitudinal (X_R) and lateral (Y_R) forces, as well as the yaw moment (N_R) can be obtained by:

$$X_R = (1-t_R)F_X \tag{19}$$

$$Y_R = (1+a_H)F_Y \tag{20}$$

$$N_R = x_R F_Y + x_H a_H F_Y \tag{21}$$

where t_R, a_H, and x_H can be seen as the coefficients describing the interaction with the hull.

In Eq. (22) x_R and x_H are the points of application of the rudder force F_Y and of the additional lateral force $a_H F_Y$. The parameters t_R, a_H, and x_H have been found to be dependent on n, u and v, see e.g. [13] for more discussion on this topic, however, in the present study, those parameters have been assumed as constant.

Wave Forces

The mean second order wave forces ($\boldsymbol{f_{2nd}}$) are important in the present study because they have a non-zero mean effect, which is crucial for the evaluation of ship's manoeuvring behaviour. These forces were obtained numerically and experimentally beforehand, and were saved as a database which was expressed as function of the wave angle of encounter μ, the ship speed V, and the wave frequency ω_{W}, see Eq. (22). In Eq. (22), in addition, a module ($\boldsymbol{F_{FK}}$) to evaluate the Froude-Krylov and hydrostatic forces is also used.

$$\boldsymbol{F}_{\mathrm{W}} = \boldsymbol{f}_{\boldsymbol{2nd}}(\mu, V, \omega_{\mathrm{W}}) + \boldsymbol{F}_{\boldsymbol{FK}} \qquad (22)$$

The numerical computations for $\boldsymbol{f_{2nd}}$ were carried out with the software package HydroStar. HydroStar is 3D potential code which can take into account the ship forward speed via the so-called "encounter-frequency" approach [8]. In addition, experiments were carried out (which are discussed further in the text) to replace the computed longitudinal mean wave forces, this as experimental values are regarded as the most accurate ones.

In important to mention that for the evaluation of the $\boldsymbol{F_{FK}}$ forces, the method is based on the discretization of the entire hull in order to compute each time step the actual wetted surface, more details on the method can be found in [7]. Bear in mind, however, that in the present study the $\boldsymbol{F_{FK}}$ forces estimation were restricted to account for the mean wetted surface only, as such they are expected to have no influence on the mean wave forces.

EXPERIMENTAL PROGRAM

The Towing Tank

The experiments were conducted at the Towing Tank for Manoeuvres in Confined Water at Flanders Hydraulics Research (FHR) in Antwerp, Belgium (in cooperation with Ghent University). The towing tank has a useful length of 68.0m, a width of 7.0m and a maximum water depth of 0.5m. It is equipped with a carriage mechanism and a wave generator, the combination of which allow to perform fully and semi-captive tests with and without wave action. More detailed information about the tank itself and the different possible test types and can be found in [16].

The Test Setup

The ship model is mounted to the carriage mechanism by means of a beam frame which is attached to the ship by pitch roll mechanism and connects to the carriage via a set of two vertical guidance systems (see Figure 1a). The setup allows semi-captive tests with the model free to move vertically and to rotate in roll and pitch. These modes of motion can be restrained independently from each other, thus allowing all possible combinations.

Time records of two composed strain gauges (LC1 and LC2) and four potentiometers (P1 to P4) are registered during tests. From these measurements forces (in surge and sway), moments (in yaw) and motions (vertical and rotations) can be derived. Wave profiles along the tank (at a fixed position) and at a constant distance from the ship (as seen by the ship) have also been recorded during tests. Two types of wave gauges have been used for this purpose: resistant type (for fixed positions) and a laser beam type (for the moving one). The position of the latter (WG1) is displayed in Figure 1. More information on the resistive type wave gauges have been omitted hereafter for the sake of brevity as they were only used to verify the wave profiles along the tank.

Note that to describe the ship position, orientation and the measurements all coordinates systems are North East Down (NED) oriented. See for instance the body fixed axes system $Oxyz$ displayed in Figure 1b.

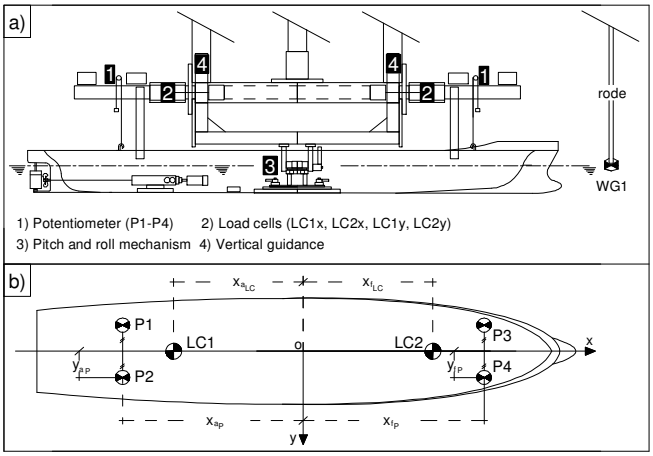

FIGURE 1: BEAM FRAME AND INSTRUMENTATION ARRANGMENT DURING TESTS, ($\boldsymbol{a}$) COUPLING BEAM FRAME, SHIP AND TANK CARRIAGE, ($\boldsymbol{b}$) POSITIONS OF INSTRUMENTS

The Ship Model

Tests were conducted with a $1/90$ scale model of an Ultra Large Container Ship (ULCS) C0W. The main characteristics are displayed in Table 1 and a profile view of the ship hull is shown in Figure 2.

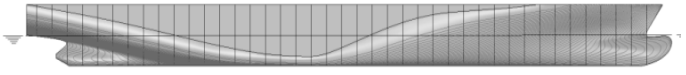

FIGURE 2: PROFILE VIEW OF THE C0W CONTAINER SHIP (ULCS). WATERLINE SHOWN AT THE DRAFT $\boldsymbol{T_m}$ OF 13.1 m

TABLE 1: CONTAINER SHIP C0W MAIN PARTICLAURS AT FULL SCALE

Item		Value	
LOA	Length over all	397.6	(m)
Lpp	Length between perpendiculars	377.2	(m)
B	Breadth	56.4	(m)
D	Depth of ship	29.7	(m)
T_m	Draft, midships	13.1	(m)
Cb	Block coefficient	0.6	$(-)$
m	Ship's mass	1.65E+5	(ton)
R_{xx}	Longitudinal radius of inertia	19.1	(m)
R_{yy}	Transverse radius of inertia	92.6	(m)
R_{zz}	Vertical radius of inertia	94.9	(m)
x_G	Longitudinal position centre of gravity	-9.7	(m)
y_G	Transverse position centre of gravity	0	(m)
z_G	Vertical position centre of gravity	0	(m)

The ship model was equipped with a single propeller and a single rudder. The propeller geometry was designed according to the Wageningen B-series with six blades; the rudder is a semi-balanced design. Figure 3 shows both of them as installed on the model. Their main particulars are given in Table 2.

FIGURE 3: SINGLE PROPELLER AND SINGLE SEMI-BALANCED RUDDER INSTALLED ON THE SHIP MODEL

TABLE 2: FULL SCALE PROPELLER AND RUDDER MAIN CHARACTERISTICS

Single propeller		Single Rudder	
Rotation	Right	Height	13.5m
Number of blades	6	Area	97.2m^2
Diameter	9.63m	-	-

Test Matrix

Two different wave amplitudes (ζ_a), 1.00 m (RW1) and 1.35 m (RW2), and seven wave lengths (λ) have been used yielding a total of 14 regular waves. The wave frequencies displayed in Table 3 have been estimated for a water depth (h) of 19.6 m corresponding to a 50% UKC. Bear in mind that the present environmental conditions are commonly met by ULCS in the coastal areas of main Belgian sea ports. Steady straight line tests with and without propeller and rudder action have also been conducted to investigate the ship resistance and wake factors. The selected ship speeds, propeller rates (n) and rudder angles (δ_R) are shown in Table 4.

The same tests have been paired with the regular waves, described above, to investigate the added wave resistance (RAW), and the influence of waves on the propeller and rudder wake factors. The chosen parameters are given in Table 5 and Table 6.

TABLE 3. FULL SCALE WAVE'S MAIN PARAMETERS ENCOUNTERED IN THE COASTAL AREAS OF THE MAIN BELGIAN SEA PORTS

$L_{PP}/\lambda(-)$	ω_W (rad/s)	ζ_A (m)
3.85	0.73	
3.13	0.63	
2.63	0.55	
2.27	0.48	1.00 (RW1), 1.35 (RW2)
2.00	0.43	
1.67	0.37	
1.43	0.32	
1.25	0.28	

TABLE 4: PROPELLER AND RUDDER TESTS IN CALM WATER. $\boldsymbol{n_0 = 105}$ RPM

$F_r\ (-)$	n/n_0 (%)	δ_R (deg)
0.050	0, 75, 100	0, 35
0.125	0, 75, 100	0, 35

TABLE 5: STEADY STRAIGTH LINE TESTS WITH REGULAR WAVES

$F_r\ (-)$	L_{PP}/λ (-)	μ (deg)
0.050	3.85, 2.63, 2.0, 1.43 (RW1)	0, 180
0.125	3.85, 2.63, 2.0, 1.43 (RW1 and RW2)	0, 180

TABLE 6: PORPELLER AND RUDDER TESTS IN REGULAR WAVES (RW1)

$F_r\ (-)$	L_{PP}/λ (-)	n/n_0 (%)	δ_R(deg)	μ(deg)
0.050	2.27,1.67,1.25	75,100	0, 35	180
0.125	2.27,1.67,1.25	75,100	0, 35	180

To study the main wave characteristics, forces and moments recorded during tests a post processing analysis was performed. The analysis was carried out based on the recommendations in [17] with respect to selection of the time windows and post processing of the harmonic signals. In this method the selected part of the signal is filter and further fitted with a least square method to a Fourier expansion up to a third order, see Eq. (23).

$$f(t) = a_0 + \sum_{i=1}^{3} a_i \cos(\omega_n t) + b_i \sin(\omega_n t) \qquad (23)$$

In Eq. (23), a_0 and ω_n are the mean and the frequency of the harmonic signals, respectively, and a_i and b_i are the first, the second, and the third order harmonics of the Fourier series. For the analysis of calm water results, the study was conducted over the same regions defined for waves. More details of the post processing analysis of the tests can be found in [7] and [18].

TEST RESULTS AND DISCUSIONS

Wave Forces: Added Resistance

The results obtained from the experimental analysis for the mean second order wave forces in surge (added wave resistance, RAW) are presented in Figure 4 and Figure 5 for head and following waves, respectively. The numerical values, obtained with the software package HydroStar, are also displayed in the figures for comparison.

From the tests results obtained in head waves, see Figure 4, it can be seen that the RAW increases as function of the speed and presents larger magnitudes for longer wave lengths, but remains approximately constant for the shorter wave lengths. The latter confirms the dependency of the second order forces on the ship motions, reported in previous literature, e.g. in deep water in [19], and in shallow water in [20] and [18].

In following waves, see Figure 5, the tests results show larger magnitudes at the larger speed and the mid-range wave lengths. This is not expected and cannot be clearly explained at this point; but one reason may be the interaction between the return current (generated by the ship moving in shallow water) and the waves, which oppose to each other hence increasing locally the wave amplitude and consequently changing the magnitude and sign of RAW. This is an important point of attention for further research.

Note as well that from the tests in head waves, Figure 4 (bottom), one can observe that the experiments conducted at two different wave amplitudes (1.00 m and 1.35 m) present approximately the same non-dimensional values. This suggest that, for the present study, the added wave resistance can be assumed proportional to the square of the wave amplitude.

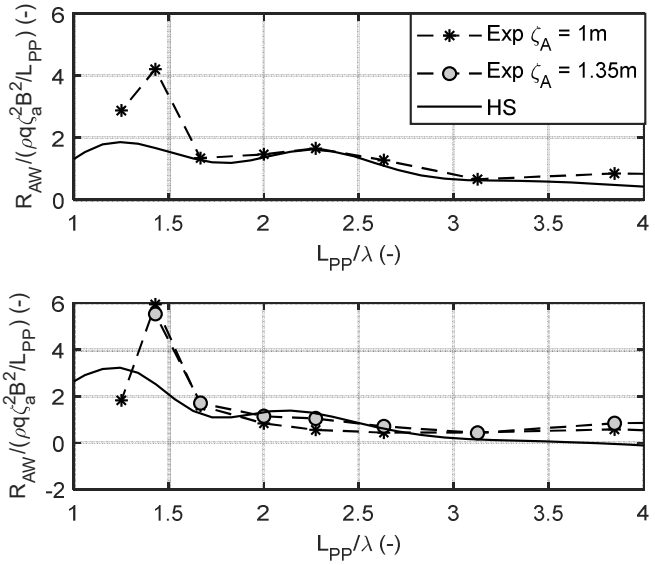

FIGURE 4: EXPERIMENTAL (EXP) AND HYDORSTAR (HS) RESULTS FOR THE ADDED WAVE RESISTANCE AT TWO SHIP SPEEDS 6KNOTS (TOP) AND 15 KNOTS (BOTTOM) OBTAINED AT TWO DIFFERENT $\boldsymbol{\zeta_A}$ OF 1.00 $\boldsymbol{m}$ AND 1.35 $\boldsymbol{m}$ IN HEAD WAVES

Comparing the tests results for both speeds in head waves with the numerical estimations (see Figure 4), it can be seen that in general a good approximation is obtained, except at the lowest and highest L_{PP}/λ ratios. In following waves, see Figure 5, discrepancies between the numerical and experimental results are even larger than in head waves, especially at the higher speed.

From these observations, one can state that the overall accuracy of numerical results is poor, being even more questionable in following waves and higher speeds. This suggest that experimental results should be preferred for further evaluation of the ship in waves. However, when experiments are not available, numerical results can still be used to fill the gaps but one should bear in mind the discrepancies encountered.

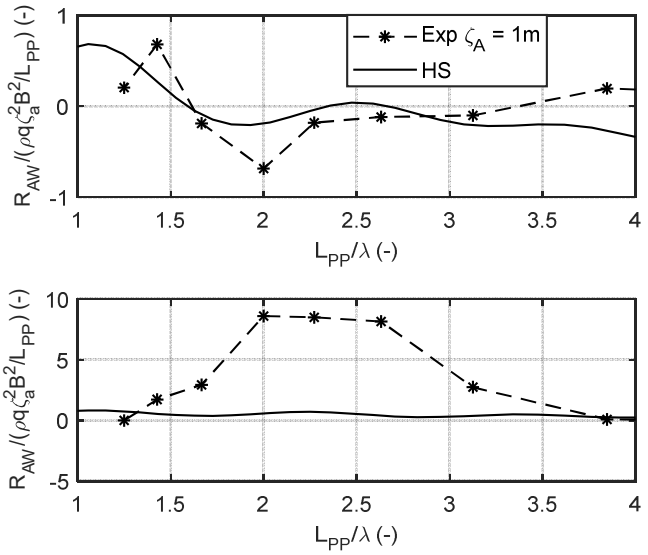

FIGURE 5: EXPERIMENTAL (EXP) AND HYDROSTAR (HS) RESULTS FOR THE ADDED WAVE RESISTANCE AT TWO SHIP SPEEDS 6KNOTS (TOP) AND 15 KNOTS (BOTTOM) OBTAINED AT $\boldsymbol{\zeta_A}$, $\boldsymbol{1.00\ m}$ IN FOLLOWING WAVES

Propulsion

The thrust coefficient K_T and the wake fraction w_T at the propeller are presented in Figure 6. The wake at the propeller was obtained by the thrust identity method.

In Figure 7 the thrust coefficient t is also shown for comparison. Note that t was obtained from captive tests, see Eq. (24), and not from free running tests at self-propulsion, as such, its validity can be questioned but as the main idea is to illustrate the rudder performance in waves, the results are still relevant.

$$t = \frac{T - (F + R)}{T} \tag{24}$$

In Eq. (24), T is the propeller thrust, R the ship resistance, and F the total longitudinal force measured during experiments.

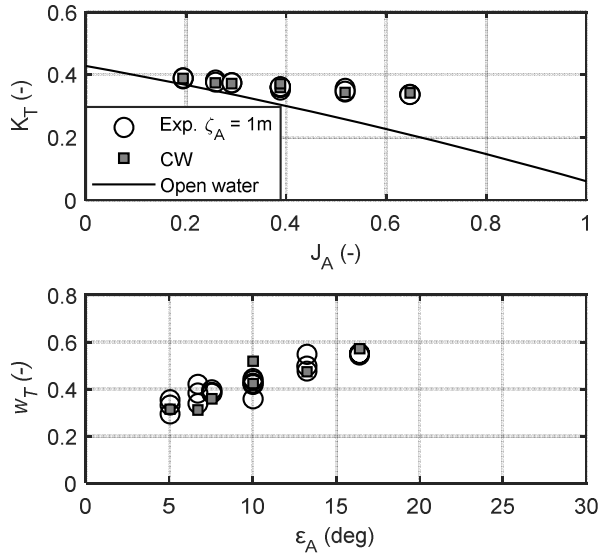

FIGURE 6: THRUST COEFFICIENT (TOP) AND WAKE FRACTION (BOTTOM) OBTAINED FROM TEST IN CALM WATER (CW) AND IN HEAD WAVES, WITH $\boldsymbol{\zeta_A}$ OF 1.00 $\boldsymbol{m}$

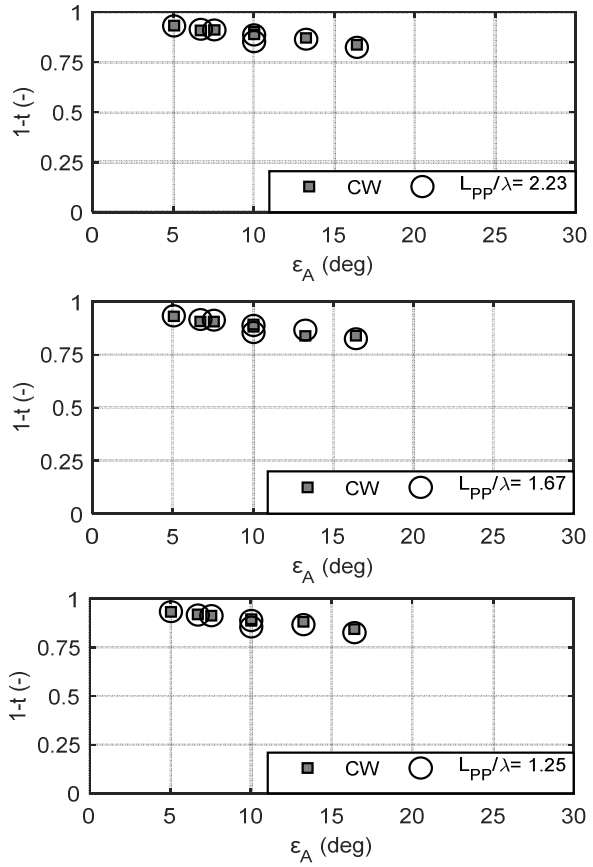

FIGURE 7: THRUST DEDUCTION COEFFICIENT OBTAINED IN CALM WATER (CW) AND IN HEAD WAVES FOR THREE DIFFERENT $\boldsymbol{Lpp/\lambda}$ RATIOS, WITH $\boldsymbol{\zeta_A}$ OF 1.00 $\boldsymbol{m}$

From Figure 6 (top) it can be observed that the magnitudes of the thrust coefficient remain approximately the same, this is reflected in the wake fraction (Figure 6, bottom) where slightly larger variations are obtained.

When looking at the thrust deduction factor t, Figure 7, similarly to what was observed for K_T and w_T in Figure 6, the results in waves remain approximately the same as the ones obtained in calm water.

The insignificant influence of the waves (studied in the present work) on the propeller performance, as seen in Figure 6 and Figure 7, indicates that with respect to the propeller performance the calm water values can still be used when shallow water waves are present.

Rudder

In Figure 8, the results obtained for the rudder wake fraction (w_{RY}) are presented. The wake was obtained with a method similar to the thrust identity method, where the lateral rudder force was used instead of the K_T curves.

It can be seen from Figure 8 that the magnitudes of w_{RY} in waves remain approximately the same as the ones obtained in calm water. Thus, the calm water results for the rudder performance can be used without much concern for the wave conditions studied in this work. This assumption, however, should be taken with care as the present observations have been found for a larger rudder angle δ_R paired with a larger propeller rate n; the same behaviour might not be observed when smaller δ_R paired with lower n are used. This remains as a topic for further research.

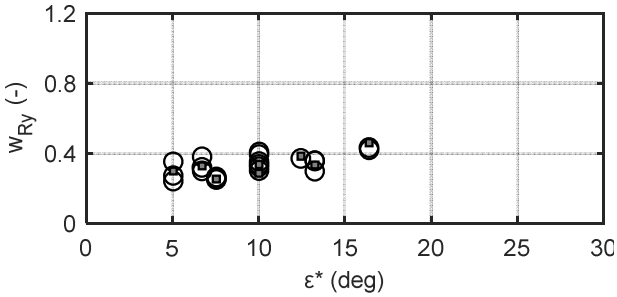

FIGURE 8: WAKE FRACTION $\boldsymbol{w_{RY}}$ OBTAINBED FOR TESTS IN CALM WATER (SQUARES) AND IN HEAD WAVES (CIRCLES) AT $\boldsymbol{\delta_R}$ OF 35 $\boldsymbol{deg}$ AND AT $\boldsymbol{\zeta_A}$ OF 1$\boldsymbol{m}$ AND $\boldsymbol{L_{PP}/\lambda}$ RATIO OF 1.25, 1.67, AND 2.23

NUMERICAL SIMULATIONS

General considerations

Note that the hull, propeller, and rudder characteristics from calm water have been obtained from [7], [17], and models available and FHR. These characteristics are not discussed in here for purposes of brevity and because of confidentiality.

In the course of the study the numerical estimation of the mean second order wave forces in sway and yaw moment showed and oscillatory behaviour when the ship forward speed was considered. This may be due to artificial approach used by

HydroStar to cope with the forward speed effect were results for the non-zero speed case are based on the zero-speed case via the encounter-frequency approximation. Thus, the mean wave forces computed at zero forward speed (see Figure 9) and assumed symmetrical with respect to the xz-plane were chosen for further evaluations of the ship's turning ability.

Note as well that the zero speed case is a good approximation for the sway force and yaw moment, this is as their magnitudes are less influenced by the ship forward speed than the surge forces. In the case of the surge forces, the numerical results were partially replaced by the experimental ones.

From the evaluation of the turning ability and further discussions of the results, the advance (x_{090}), the transfer (y_{090}), the tactical diameter (y_{0180}) and a drift (β_{TC}) angle are defined as shown in Figure 10. β_{TC} indicates the direction where the turning circle deviates with respect to calm water and it is defined by the three points, (x_{090}, y_{090}), (x_{0450}, y_{0450}), and (x_{0810}, y_{0810}).

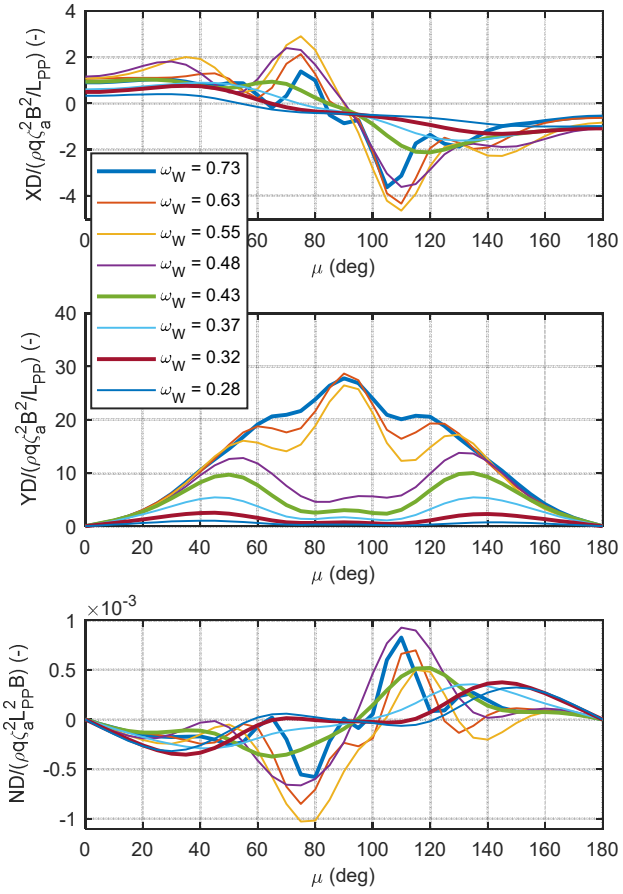

FIGURE 9: MEAN SECOND ORDER WAVE FORCES IN SURGE (TOP), SWAY (MIDDLE) AND YAW MOMENT (BOTTOM) OBTAINED WITH HYDROSTAR AT ZERO SPEED

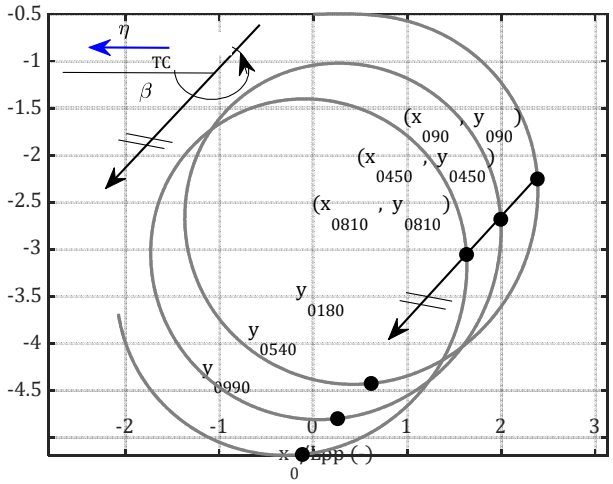

FIGURE 10: DEFINITION OF THE TURNING CIRCLE MAIN CHRACTERISTICS, EXAMPLE IN WAVES ($\boldsymbol{\eta = 180\ deg}$)

Wave effects of the Turning Circle in Shallow Water

In Figure 11, Figure 12, and Figure 13 the turning circle trajectories obtained for three different Lpp/λ ratios, 3.85, 2.00, and 1.43, respectively, are presented. In the figures, the calm water results are also displayed for comparison.

The turning circles were evaluated for a wave amplitude of 1.35 m, rudder angle of 35 deg, and a fixed propeller rate of $75\%n_0$ and for three different wave angles. The cases where the wave angles are 0 deg, 90 deg, and 180 deg are hereafter referred as following (FW), beam (BW) and head seas (HW), respectively, for brevity purposes. It is worth mentioning that the propeller rate of $75\%n_0$ is needed to achieve, in calm water, the self-propulsion point for a speed of 15 knots.

From Figure 11, for all simulations in waves, one can observe a drifting of the ship's trajectory with respect to the calm water results caused by the wave drift forces. In each case, the drifting direction is not parallel to the wave direction and defines an angle with the wave main direction. The latter has also been reported in several works which indicates that the solutions of the present study are consistent, see e.g. [3], [21].

Note that from all simulations, an oscillatory behaviour of the ship's trajectory can be observed for all cases, this is more visible for following waves because of the continuous line chosen to plot the results. This oscillatory behaviour is due to a module ($\boldsymbol{F_{FK}}$) designed to compute the actual Froude-Krylov and hydrostatic forces. Bear in mind that for the present study the $\boldsymbol{F_{FK}}$ forces were computed only on the mean wetted surface.

From Figure 11 to Figure 13 a change in the direction of the developed turning circles is observed. This change seems to be dependent on the wave drift moment in yaw (see, Figure 9) which for the shorter waves presents a higher peak around 90 deg incoming wave angle, and being almost zero for the longer waves.

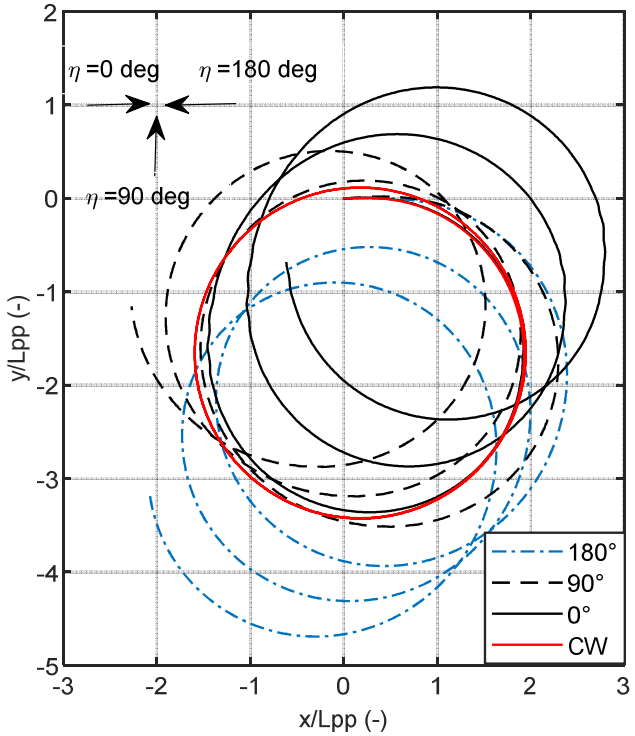

FIGURE 11: TURNNING CIRCLE IN CALM WATER (CW) AND IN WAVES AT $\boldsymbol{\eta = 0\,deg}$, $\boldsymbol{\eta = 90\,deg}$, $\boldsymbol{\eta = 180\,deg}$, $\boldsymbol{\zeta_A = 1.35m}$, $\boldsymbol{Lpp/\lambda = 3.85}$, $\boldsymbol{\delta_R = 35\,deg}$, AND $\boldsymbol{n = 75\%n_0}$

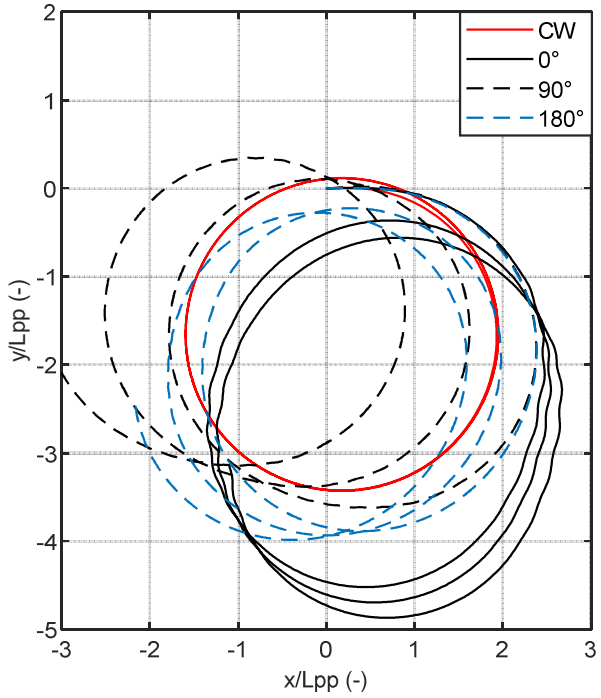

FIGURE 12: TURNNING CIRCLE IN CALM WATER (CW) AND IN WAVES AT $\boldsymbol{\eta = 0\,deg}$, $\boldsymbol{\eta = 90\,deg}$, $\boldsymbol{\eta = 180\,deg}$, $\boldsymbol{\zeta_A = 1.35m}$, $\boldsymbol{Lpp/\lambda = 2.00}$, $\boldsymbol{\delta_R = 35\,deg}$, AND $\boldsymbol{n = 75\%n_0}$

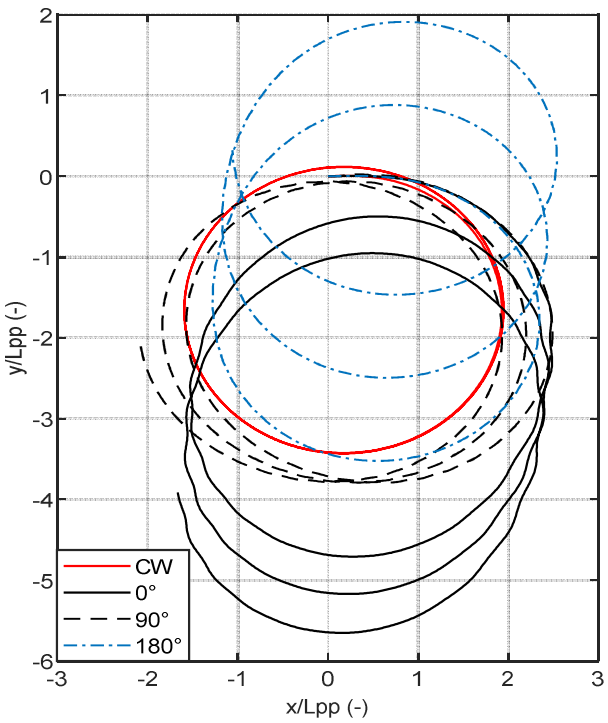

FIGURE 13: TURNNING CIRCLE IN CALM WATER (CW) AND IN WAVES AT $\boldsymbol{\eta = 0\,deg}$, $\boldsymbol{\eta = 90\,deg}$, $\boldsymbol{\eta = 180\,deg}$, $\boldsymbol{\zeta_A = 1.35m}$, $\boldsymbol{Lpp/\lambda = 1.43}$, $\boldsymbol{\delta_R = 35\,deg}$, AND $\boldsymbol{n = 75\%n_0}$

Another important observation is that the turning circle in Figure 11 presents a smaller area covered in comparison to the ones observed in Figure 12 and Figure 13. The reason behind this, to the authors opinion, lies in the larger added wave resistance experienced by the ship at mid-range wave lengths when attaining the condition of head and following waves (see Figure 4 and Figure 5), which is not the case for the longer and shortest wave lengths where negligible values are obtained.

From the different executed simulations, the turning circle main characteristics for the advance, the transfer and the tactical diameter (as defined in Figure 10) are presented in Table 7. From Table 7 it can be seen that the advance and the transfer parameters remain approximately constant, in contrast to the tactical diameter (y_{0180}/L_{PP}). The scenarios where the latter increases the most are found at mid and longer wave lengths in following waves. At these conditions an increment of 22% ($y_{0180}/L_{PP} = 4.5$) to 27% ($y_{0180}/L_{PP} = 4.7$) with respect to calm water results. These larger changes in tactical diameter can be associated, partially, to the larger magnitudes of the added wave resistance as discussed above (see also Figure 4 and Figure 5) and the differences between the two results (mid and long wave length) to the magnitudes of the sway and yaw wave drift forces.

Bear in mind that the results can be questioned as no validation was carried out. In spite of that, the results are still representative for the present investigation as the purpose is mainly to investigate the influence of waves on the turning circle in shallow water. The validation remains as the main task of further study.

TABLE 7: TURNIG CIRCLE CHARACTERISTICS IN CALM WATER (CW), IN FW ($\boldsymbol{\eta = 0\ deg}$), IN BW ($\boldsymbol{\eta = 90\ deg}$), AND IN HW ($\boldsymbol{\eta = 180\ deg}$), AT $\boldsymbol{\zeta_A = 1.35\ m}$, $\boldsymbol{\delta_R = 35\ deg}$, AND $\boldsymbol{n = 75\%\ n_0}$

Item	L_{PP}/λ	x_{090}/L_{PP}	y_{090}/L_{PP}	y_{0180}/L_{PP}	β_{TC}
CW	-	2.4	1.7	3.7	-
FW	3.85	2.4	1.6	3.7	50
BW	3.85	2.3	1.6	3.5	322
HW	3.85	2.4	1.8	3.9	46
FW	2.00	2.5	1.8	4.5	297
BW	2.00	2.4	1.6	3.6	343
HW	2.00	2.4	1.7	3.9	9
FW	1.43	2.5	1.9	4.7	84
BW	1.43	2.5	1.7	3.8	2
HW	1.43	2.3	1.6	3.5	85

CONCLUSIONS

The present study investigates the influence of waves on the turning ability of an ultra large container ship in shallow water. Experimental investigations have been conducted in order to verify if the main assumptions of the two time scale method, where oscillatory behaviour of waves have no significant influence on the performance of the rudder and the propeller. This was confirmed in the present study for the range of waves taken into consideration.

The investigation shows that the drift of the turning circle with respect to the calm water results depends on the wave length and the direction of drift may be in opposite direction for longer and shorter wave lengths. Moreover, it was also found that the most critical characteristics affected are the tactical diameter while the advance and the transfer remains approximately the same. With respect to the direction of the waves the cases defined as following waves were found to be as the ones were a significant change of the tactical diameter is obtained, however, this is only applied to the mid and long wave length range.

FUTURE WORK

The validation of the turning ability in waves remains as the main task for further study, as well as the investigation of the applicability of other methods, such as the Rankine panel method, for the estimation of the mean second order wave forces and moments. Furthermore, the influence of squat effects on the manoeuvring behaviour in waves will be investigated.

REFERENCES

[1] P. A. Bailey, W. C. Price, and P. Temarel, "A unified mathematical model describing the manoeuvring of a ship travelling in a seaway," RINA, vol. 140, pp. 131–149, 1998.

[2] R. Skejic and O. M. Faltinsen, "A unified seakeeping and maneuvering analysis of ships in regular waves," J. Mar. Sci. Technol., vol. 13, no. 4, pp. 371–394, 2008.

[3] M.-G. Seo and Y. Kim, "Numerical analysis on ship maneuvering coupled with ship motion in waves," Ocean Eng., vol. 38, no. 17–18, pp. 1934–1945, 2011.

[4] V. Ankudinov, "Simulation analysis of ship motion in waves," in In: Proceedings of the International Workshop on Ship and Platform Motions, 1983.

[5] K. J. Schoop-zipfel, "Efficient Simulation of Ship Maneuvers in Waves," Hamburg University of Technology, 2016.

[6] W. Zhang, Z. J. Zou, and D. H. Deng, "A study on prediction of ship maneuvering in regular waves," Ocean Eng., vol. 137, no. March, pp. 367–381, 2017.

[7] M. Tello Ruiz, "Manoeuvring model of a container vessel in coastal waves," Ghent University, 2018.

[8] Bureau Veritas, HYDROSTAR for experts user manual, 2012.

[9] G. Delefortrie, K. Eloot, E. Lataire, W. Van Hoydonck, and M. Vantorre, "Captive model tests based 6 DOF shallow water manoeuvring model," in *4th MASHCON*, pp. 273–286, 2016.

[10] K. Kijima, "Manoeuvrability of ship in confined water," in International Conference on Ship Manoeuvrability, pp. 1–15, 1987.

[11] E. Kobayashi, "A simulation study on ship manoeuvrability at low speeds," in International Conference on Ship Manoeuvrability-Prediction and Achievement, 1987.

[12] M. Vantorre and K. Eloot, "Hydrodynamic phenomena affecting manoeuvres at low speed in shallow navigation areas," in 11th International Harbour Congress, 1996, pp. 535–546.

[13] G. Delefortrie, "Manoeuvring Behaviour of Container Vessels in Muddy Navigation Areas," Ghent University, 2007.

[14] M. Vantorre, Nauwkeurigheidsoverwegingen en optimalisatie van de parameterkeuze bij gedwongen maneuvreerproeven met scheepsmodelen. Ghent, Belgium: Ghent University, 1989.

[15] J. Brix, Manoeuvring technical manual, Seehafen V. Seehafen Verlag GmbH, 1993.

[16] G. Delefortrie, S. Geerts, and M. Vantorre, "The towing tank for manoeuvres in shallow water," in *4th MASHCON*, pp. 226–235, 2016.

[17] M. Tello Ruiz, M. Mansuy, G. Delefortrie, and M. Vantorre, "Manoeuvring study of a container ship in shallow water waves," in Proceedings of the ASME 2018 37th International Conference on Ocean, Offshore and Arctic Engineering OMAE2018, 2018.

[18] M. Tello Ruiz, M. Mansuy, G. Delefortrie, and M. Vantorre, "Modelling the manoeuvring behaviour of an ULCS in coastal waves," Ocean Eng., vol. 172, pp. 213–233, 2019.

[19] J. Strom-Tejsen, H. Y. . Yeh, and D. D. Moran, "Added resistance in waves," SNAME, vol. 81, 1973.

[20] J. A. Pinkster and R. H. M. Huijsmans, "Wave drift forces in shallow water," Behav. offshore Struct. BOSS, pp. 1159–1183, 1992.

[21] H. Yasukawa, "Maneuvering simulation of a KVLCC2 tanker in irregular waves," in MARSIM2015, 2015.